

INFLUENCE OF WATER PURIFICATION COAGULANT RESIDUE ON THE STRENGTH AND FREEZE-THAW RESISTANCE OF CONCRETE BRICKS

TAIJUN TIAN*, SUNWEN LIU*, YUAN CHEN*, ZHE ZHOU*, XIAOWEI GUO*, ZAN TAN*, #WEI SHI**

*China Communications Road and Bridge Construction Co., Ltd., Beijing 101107, China

**School of Civil Engineering, Henan Polytechnic University, Jiaozuo 454002, China

#E-mail: no1body323@outlook.com

Submitted October 22, 2025; accepted March 23, 2026

Keywords: Water treatment coagulant residue, Cement substitution, Pozzolanic reactivity, Freeze-thaw cycling, Pore structure, Dry pressing, Industrial solid-waste utilization

To realise the resource-oriented utilisation of poly-aluminium chloride (PAC) residue rich in SiO_2 and Al_2O_3 , the residue was dechlorinated, dried, and used to partially replace cement by mass to fabricate static-press concrete bricks. The compressive and flexural strengths at 28 days and durability after 50 freeze-thaw cycles were tested, and a microstructural characterisation was performed by X-ray fluorescence (XRF), X-ray diffraction (XRD), and scanning electron microscopy (SEM). The results show that, after pre-treatment, the cumulative content of SiO_2 and Al_2O_3 in the PAC residue reaches 73.52 %, confirming its potential as a reactive pozzolanic material. When the replacement ratio is ≤ 20 %, the 28-day compressive strength remains 85 – 95 % of the control, and the strength loss after 50 cycles is below 20 %, meeting specific standards. At replacement ratios > 20 %, both the mechanical and durability performances decline markedly. The microstructural analysis suggests that, at low replacement ratios, the residue refines the pore structure via microaggregate effects and secondary hydration, whereas at high levels, dilution effects and residue morphology increase the porosity. This verifies the feasibility of PAC residue (≤ 15 % replacement) in static-press bricks and provides guidance for its industrial valorisation in green building materials.

INTRODUCTION

Poly-aluminium chloride (PAC), as a high-efficiency water-treatment flocculant, exhibits clear advantages over conventional coagulants in treatment efficiency [1] and flocculation performance [2, 3], with rapid settling rates and strong adaptability [4-6], leading to its widespread application in water purification [7, 8]. PAC can be produced by various methods [9, 10]; one common process is the two-step acid leaching of bauxite and calcium aluminate, which yields liquid PAC and generates a residue rich in SiO_2 , Al_2O_3 , CaO , and other components [11].

PAC's high molecular weight and strong adsorption capacity confer superior turbidity removal compared to traditional coagulants such as alum. In an aqueous solution, PAC rapidly forms flocs that settle quickly across a broad pH range (approximately 5.0 – 9.0) at low doses. Spray-dried PAC products exhibit good stability, fast hydrolysis, and dense floc formation, resulting in low effluent turbidity and excellent dewatering characteristics [12]. These properties have underpinned the extensive application of PAC in treating both potable and industrial wastewaters.

Due to the weak acidity of PAC residue, neutralisation pre-treatment is a prerequisite for its valorisation. Research has shown that treatment with slaked lime or other alkaline agents, followed by stirring, dewatering, and low-temperature calcination, effectively removes the chloride ions and acidic components. Kim et al. [13] neutralised and dewatered PAC sludge and then applied low-temperature calcination to form granules, which markedly reduced the chloride and acidic species while enabling high As(V) adsorption. Li et al. [14] further showed that incorporating Portland blast-furnace slag cement and bentonite into the PAC residue effectively neutralises the acidity and enhances the mechanical performance of the resulting stabilised material, providing an alternative to conventional lime-based treatment. Building on the compositional evidence, Xu et al. [15] identified PAC slag as chemically akin to aluminosilicate industrial residues (e.g., polyferric sulfate waste, red mud) [16], with silica (SiO_2) and alumina (Al_2O_3) as the dominant phases. Consistent with this, Wang et al. [17] reported that the reactive SiO_2 and Al_2O_3 in PAC slag drive the pozzolanic reactions in cementitious systems. Quantitatively, Yang et al. [18] measured 45.72 % SiO_2 and 27.80 % Al_2O_3 in the PAC residue, confirming its pozzolanic character.

Following appropriate pre-treatments - such as water washing and low-temperature calcination - the reactivity of PAC slag is further enhanced, supporting its use as a supplementary cementitious material to contribute to the hydration and refine the concrete microstructure. Drawing on analogous studies of industrial wastes [19, 20], PAC residue shows promise as a cement-replacement material [21]. The partial cement substitution with PAC residue not only mitigates environmental pollution [22, 23], but also reduces the cement consumption, offering significant economic and social benefits [24, 25].

Incorporating industrial solid wastes into cementitious matrices can, however, affect the mechanical properties, pore structure, and moisture transport, thereby influencing the freeze-thaw durability. Prior work has demonstrated that ~ 20 % fly-ash replacement can mitigate the mass loss and preserve the dynamic elastic modulus under freeze-thaw cycles [26]; that blast-furnace slag activated with metakaolin forms dense C-A-S-H/N-A-S-H gels, reducing the porosity and impeding the water migration to enhance the freeze-thaw performance [27]; and that activated zeolite-slag geopolymer systems continue to densify under ambient and freeze-thaw conditions, improving resistance [28]. High-fly-ash mixes, when the air content and curing are optimised, limit the liquid uptake and crack propagation during freeze-thaw, boosting durability [29]; and adjusting the metakaolin content with alkaline activator ratios can precisely control the pore-size distribution, balancing the early strength with the long-term freeze-thaw resilience [30]. These findings offer guidance for the mix designs and microstructural optimisation when substituting PAC residue (rich in SiO_2 and Al_2O_3) into concrete bricks, enabling the assessment of the mechanical and durability evolution across replacement levels and the elucidation of the underlying mechanisms.

Following the pre-treatment and compositional analysis of the PAC residue, concrete bricks were fabricated using various replacement ratios. Their 28-day compressive and flexural strengths, along with their durability after 50 freeze-thaw cycles, were systematically evaluated. The influence of the PAC-residue incorporation on the mechanical performance and freeze-thaw resistance was investigated, and micro-structural characterisations (XRF, XRD, SEM) were used to elucidate the underlying mechanisms of the PAC-residue addition in the brick matrix.

This study provides both experimental data and theoretical insights for the development of concrete bricks containing PAC residue, facilitating the resource-oriented utilisation of this industrial by-product and reducing environmental pollution from residue disposal.

EXPERIMENTAL

Experimental materials and PAC residue pre-treatment *Experimental materials*

P.O. 42.5 ordinary Portland cement was used. The fine aggregate was manufactured sand with a fineness modulus of 2.7, conforming to the “Aggregates for Construction—Sand for Construction” (GB/T 14684-2011) standard. The coarse aggregate was crushed stone per “Aggregates for Construction—Pebble and Crushed Stone” (GB/T 14685-2011), in two size fractions (2.36 – 4.75 mm and 4.75 – 9.5 mm), with an apparent density of $\approx 2652 \text{ kg}\cdot\text{m}^{-3}$, and a crushing value of 6.9 %. The mixing water was ordinary tap water; the water-reducing admixture was a high-performance polycarboxylate superplasticiser. These aggregates were used throughout the mix design and testing programme.

Selection of PAC residue and dechlorination treatment

The poly-aluminium chloride (PAC) residue used in this study was sourced as an industrial by-product from a water-treatment agent manufacturing facility located in Henan Province, China. Owing to its weak acidity, the raw residue cannot be used directly as a cementitious additive. As illustrated in Figure 1, the collected PAC residue was mixed with quicklime (CaO) and then blended with water to form a slurry, which was stirred to promote a homogeneous reaction.

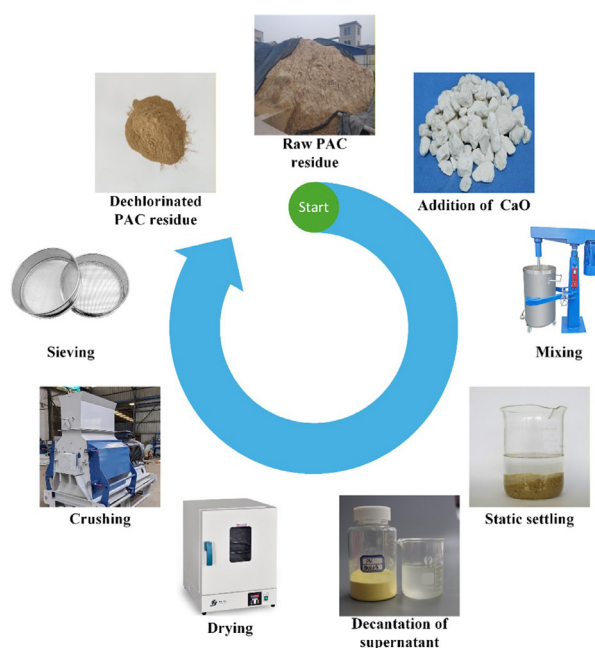


Figure 1. Flowchart of the dechlorination treatment process for PAC residue.

Table 1. Mix proportions for the specimen preparation.

Mix ID	Material quantity per unit volume ($\text{kg}\cdot\text{m}^{-3}$)				
	Cement	Water	Cement	Fine Aggregate	Cement
A0	360	A0	360	A0	360
A10	324	A10	324	A10	324
A15	306	A15	306	A15	306
A20	288	A20	288	A20	288
A25	270	A25	270	A25	270
A30	252	A30	252	A30	252

After preparation, the slurry was allowed to stand for natural sedimentation, separating the supernatant from the settled residue. The supernatant rich in calcium chloride (CaCl_2) and residual slaked lime ($\text{Ca}(\text{OH})_2$) was decanted to remove the soluble chloride ions and acidic components. The settled residue was dried to reduce the remaining chlorides and acidity, then crushed, sieved, and ground to produce the test-grade material.

Preparation of concrete brick specimens

The control mixture (A0) was designed with a fixed water-to-binder (w/b) ratio of 0.40, comprising cement, fine aggregate, and coarse aggregate in a mass ratio of 1:3.4:1.45. Based on this reference, the cement was partially substituted with dechlorinated PAC residue at ratios of 0, 10, 15, 20, 25, and 30 % by weight. The detailed mix proportions per cubic meter are summarised in Table 1.

The control mix for the dry-press concrete bricks contained 16 % cement, 58 % fine aggregate, and 25 % coarse aggregate by mass. The mixing water was calculated based on a water-to-binder (w/b) ratio of 0.40. While maintaining a constant control mix (A0), the cement was partially substituted by dechlorinated PAC residue on an equal-mass basis at replacement levels of 0, 10, 15, 20, 25, and 30 %. The material quantities per unit volume are listed in Table 1.

Specimens were fabricated using the cement-coating mixing (CCM) method to optimise the interface between the aggregates and the cementitious paste. Initially, the aggregates were dry-mixed before 70 % of the total mixing water was introduced to ensure thorough pre-wetting. Subsequently, the cementitious materials (cement and PAC residue) were added and blended for 60 seconds to encapsulate the aggregate particles within a reactive precursor layer. The remaining water was then added and mixed to plasticise the matrix, followed by a final homogenisation phase.

The fresh mixtures were cast into $200 \times 100 \times 60$ mm moulds and subjected to static pressing using a GEOMECH-P-1000 hydraulic press. A slow, uniform load was applied and maintained for a specific dwell time to ensure structural density. Following a 24-hour in-mould curing period under plastic film, the specimens



a)



b)

Figure 2. Appearance of the concrete bricks.

were demoulded and transferred to a standard curing chamber (20 ± 2 °C, RH > 90 %). The mechanical properties and durability assessments were conducted at curing ages of 7 and 28 days.

Test methods

Compressive strength test

The compressive strength was determined in accordance with the GB 28635-2012 standard (Concrete Pavement Bricks). Prior to testing at the specified ages, the specimens were pre-conditioned by immersion in room-temperature water for 24 hours, followed by surface-drying to achieve a saturated-surface-dry (SSD) state. A universal testing machine was employed to apply a constant loading rate of $0.5 \text{ MPa}\cdot\text{s}^{-1}$ until

failure. To ensure the experimental reproducibility and statistical significance, three replicates were tested for each mix proportion and curing age, and the average values were recorded.

The compressive strength C (MPa) was calculated as:

$$C = \frac{P}{A} \quad (1)$$

where P is the peak load at failure (kN) and A is the loaded area (mm²).

Freeze-thaw test

The freeze-thaw durability was evaluated following the method in GB 28635-2012. After the specified number of cycles, the specimens were inspected visually, weighed, and tested for their compressive strength. The mass loss rate Δm_n and compressive-strength loss rate ΔC_n after n cycles were calculated as:

$$\Delta m_n = \frac{m_0 - m_n}{m_0} \times 100\% \quad (2)$$

$$\Delta C_n = \frac{C_0 - C_n}{C_0} \times 100\% \quad (3)$$

where m_0 and m_n are the specimen masses (kg) before testing and after n cycles, respectively; C_0 is the initial compressive strength (MPa) measured at 28 days of standard curing (prior to the freeze-thaw cycling); C_n is the compressive strength (MPa) after n cycles.

Physical and microstructural analysis of the PAC residue

The chemical composition of the dechlorinated PAC residue was measured using a Bruker S8 TIGER X-ray fluorescence spectrometer (XRF). The phase identification was performed by X-ray diffraction (Bruker D8 Advance, XRD). The microstructural morphology was examined using a field-emission scanning electron microscope (FESEM, Merlin Compact, Carl Zeiss NTS GmbH, Germany). Prior to observation, the fractured specimens were vacuum-dried and sputter-coated with a thin layer of gold to ensure an adequate electrical conductivity. The results from these analyses were used to elucidate the effects of the PAC residue on the concrete-brick microstructure.

RESULTS AND DISCUSSION

Chemical and mineralogical characteristics of the pre-treated PAC residue

Chemical composition

After dechlorination and drying, the chemical composition of the PAC residue was determined by XRF (Table 2). The major oxides - SiO₂ and Al₂O₃ -account for 45.72 and 27.80 % of the total mass, respectively, summing to over 73 %. The residual chloride (Cl) remains at approximately 2.25 %, indicating that although the pre-treatment substantially reduces the Cl, the content still exceeds the limit for ordinary concrete applications.

Mineralogical composition

The X-ray diffraction (XRD) pattern of the dechlorinated PAC residue is shown in Figure 3. A broad amorphous hump is observed, indicating that the sample is predominantly amorphous in nature. Crystalline phases

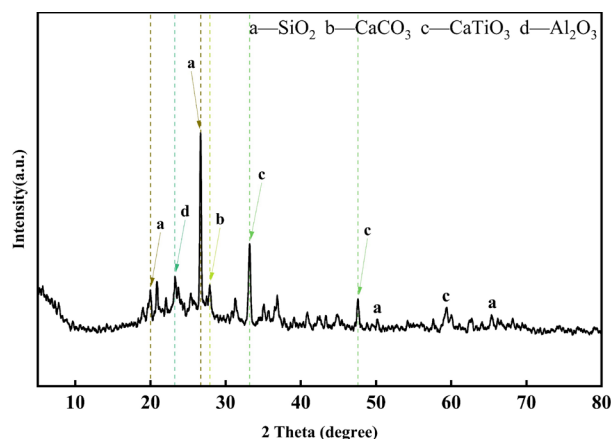


Figure 3. XRD pattern of the dechlorinated PAC residue.

such as calcium carbonate (CaCO₃) and calcium titanate (CaTiO₂) are also identified by their distinct peaks.

Peaks corresponding to SiO₂ and Al₂O₃ are present but significantly weakened. Combined with a prominent amorphous halo, this suggests that the majority of silicon and aluminium components within the residue exist in a disordered, non-crystalline state. The high proportion of amorphous aluminosilicate materials provides the potential basis for the pozzolanic activity.

Table 2. Chemical composition of the dechlorinated PAC residue (wt. %).

Component	SiO ₂	Al ₂ O ₃	Fe ₂ O ₃	CaO	MgO	TiO ₂	Cl	Others
PAC	45.721	27.80	3.42	5.675	1.34	3.855	2.25	10.389

Mechanical properties
Influence of the PAC residue content
on the compressive strength of the concrete bricks

As illustrated in Figure 4, a monotonic decrease in both the 7-day and 28-day compressive strengths was observed as the cement replacement ratio increased. The reference group (A0) exhibited the highest 28-day strength of 65.2 MPa. Upon replacing the cement with the PAC residue at levels of 10 to 30 %, the 28-day strength diminished by 7.8, 27.8, 28.8, 37.6, and 36.9 %, respectively. Notably, the strength reduction remained marginal (less than 8 %) at a 10 % replacement level, suggesting that the pozzolanic activity of the amorphous aluminosilicates in the PAC residue partially compensated for the dilution of the cement clinker. However, beyond the 10 % substitution, the strength decline became more pronounced, characterised by identifiable performance intervals between the 15 – 20 % and 25 – 30 % replacement ranges.

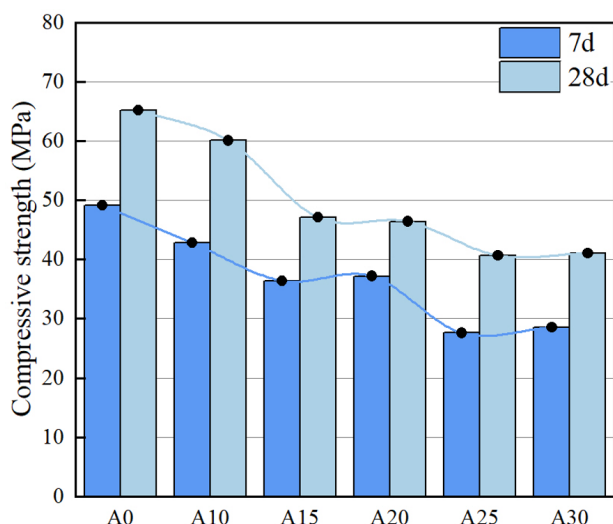


Figure 4. Effect of the PAC residue content on the compressive strength of the concrete bricks.

Influence of the PAC residue content
on the flexural strength of the concrete bricks

Figure 5 shows that, as the percentage of cement replaced by PAC residue increases, the flexural strength of the static-pressed concrete bricks decreases. In this study, the control group (A0) had a 28-day flexural strength of 7.26 MPa. When replacing the cement with the PAC residue at 10, 15, 20, 25, and 30 %, the flexural strengths dropped to 6.72, 5.44, 5.04, 4.46, and 3.80 MPa, respectively. These correspond to strength reductions of 7.4, 25.1, 30.6, 38.6, and 47.7 %, respectively. The results suggest that, at low replacement levels

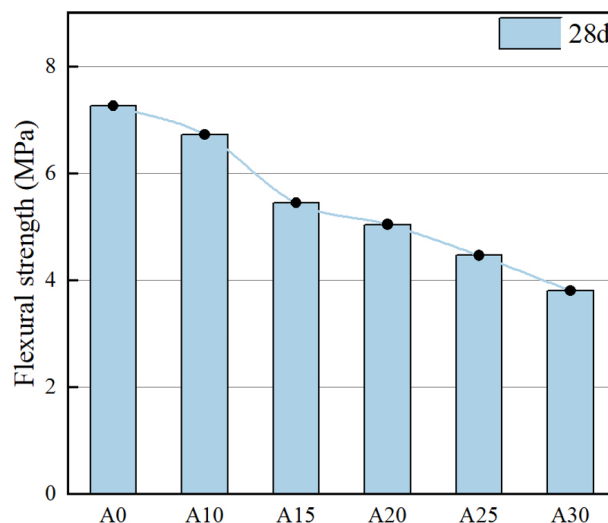


Figure 5. Flexural strength of the concrete bricks with varying PAC residue replacement levels.

($\leq 10\%$), the decrease in flexural strength is limited, whereas higher replacement levels ($> 15\%$) lead to a more significant decline.

From the mechanical strength tests conducted on concrete specimens with varying PAC residue contents, it is concluded that incorporation below 10 % exerts a negligible influence on the concrete brick strength. Although at low dosages, the pozzolanic reaction between the PAC residue and cement hydration products, together with micro-aggregate filling, can partially enhance the density and strength of the cementitious matrix, increasing the residue content leads to significant water absorption by the residue. This results in a stepwise deterioration of the workability and, consequently, reduced density of the concrete bricks, intensifying the strength loss. In summary, to balance the load-bearing performance and the resource-oriented utilisation of PAC residue, it is recommended that the replacement ratio of cement by PAC residue be kept below 15 %; beyond this threshold, adjustments to the mix design and process parameters are required.

Influence of the PAC residue content
on the freeze-thaw performance of the concrete bricks

Figure 6 shows that, after 25, 35, and 50 freeze-thaw cycles, the mass loss rate of the specimens increases with the PAC residue content. When the replacement ratio increases from 0 to 10, 15, 20, 25, and 30 %, the mass loss after 25 cycles shows an upward trend; similar patterns are observed after 35 and 50 cycles. However, for groups A0 through A20 (replacement ratios $\leq 20\%$), the mass loss rate remains within the acceptable limits of the standards even after 50 cycles.

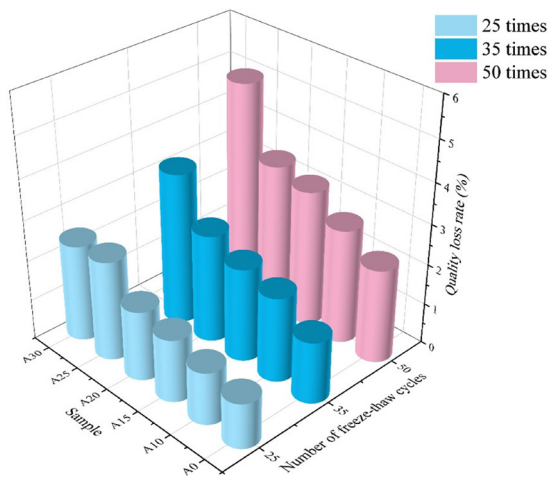


Figure 6. Mass loss rate of the PAC residue-incorporated concrete bricks under freeze-thaw cycles.

Figure 7 demonstrates that the compressive strength loss rate under freeze-thaw cycling increases proportionally with the PAC residue content. The reference group (A0) exhibited a minimal strength loss of 2.65 % after 50 cycles. In contrast, for the replacement ratios of 10, 15, 20, 25, and 30 %, the corresponding strength losses after 50 cycles were 5.69, 13.94, 17.53, 27.41, and 33.12 %, respectively (note that the 30 % group exceeded the 20 % standard limit at only 25 cycles).

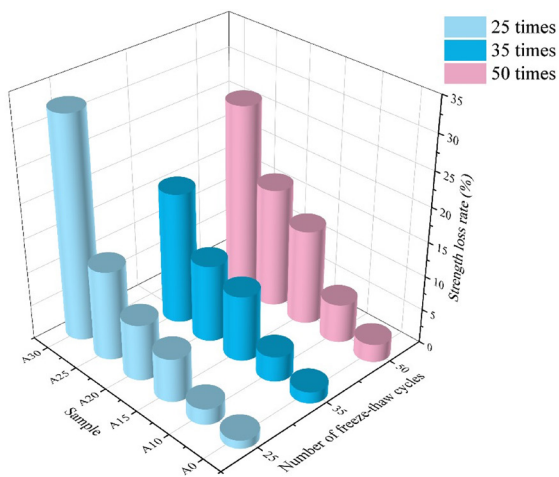


Figure 7. Strength loss rate of the PAC residue-incorporated concrete bricks under freeze-thaw cycles.

These results indicate that when the replacement ratio is maintained at or below 20 %, the strength loss remains within the permissible 20 % threshold defined by the standard. Beyond this limit, the deterioration accelerates significantly, characterising poor frost resistance. This is primarily attributed to the increased porosity and capillary water absorption in high-dosage

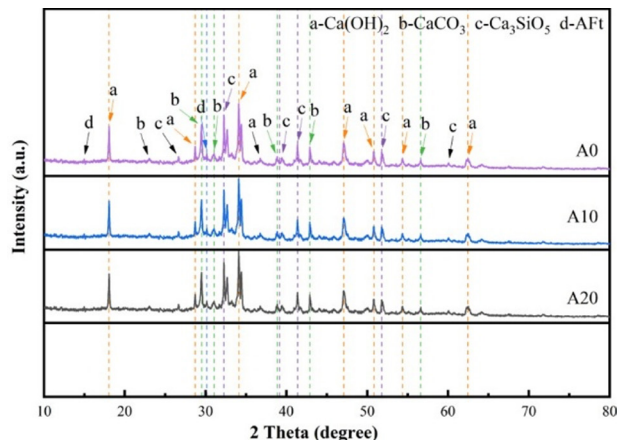


Figure 8. XRD patterns of the A0, A10 and A20 pastes at 7 days.

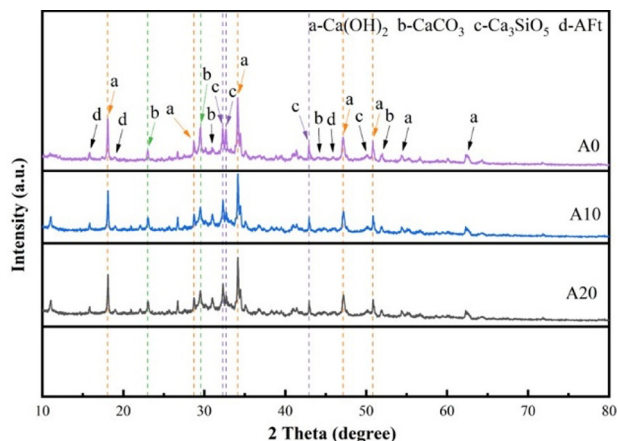


Figure 9. XRD patterns of the A0, A10 and A20 pastes at 28 days.

specimens, which amplify the internal hydraulic and ice crystallisation pressures. Consequently, these stresses initiate microcrack propagation, leading to the rapid decline in the structural integrity of the cementitious matrix. To ensure long-term durability, the cement replacement ratio should be optimised at 20 %, provided that supplementary adjustments to the mix design are implemented.

Comparison of the XRD-detected hydration products in the cement pastes with varying PAC residue contents

The X-ray diffraction (XRD) profiles in Figures 8 and 9 illustrate the phase assemblages of the reference paste (A0) compared to those incorporating 10 % (A10) and 20 % (A20) dechlorinated PAC residue. In all three systems, the primary crystalline hydration products are identified as portlandite ($\text{Ca}(\text{OH})_2$), ettringite (AFt), and residual alite (C_3S), complemented by minor calcite (CaCO_3) resulting from atmospheric carbonation. The presence of calcium silicate hydrate (C-S-H) is inferred from the amorphous background charac-

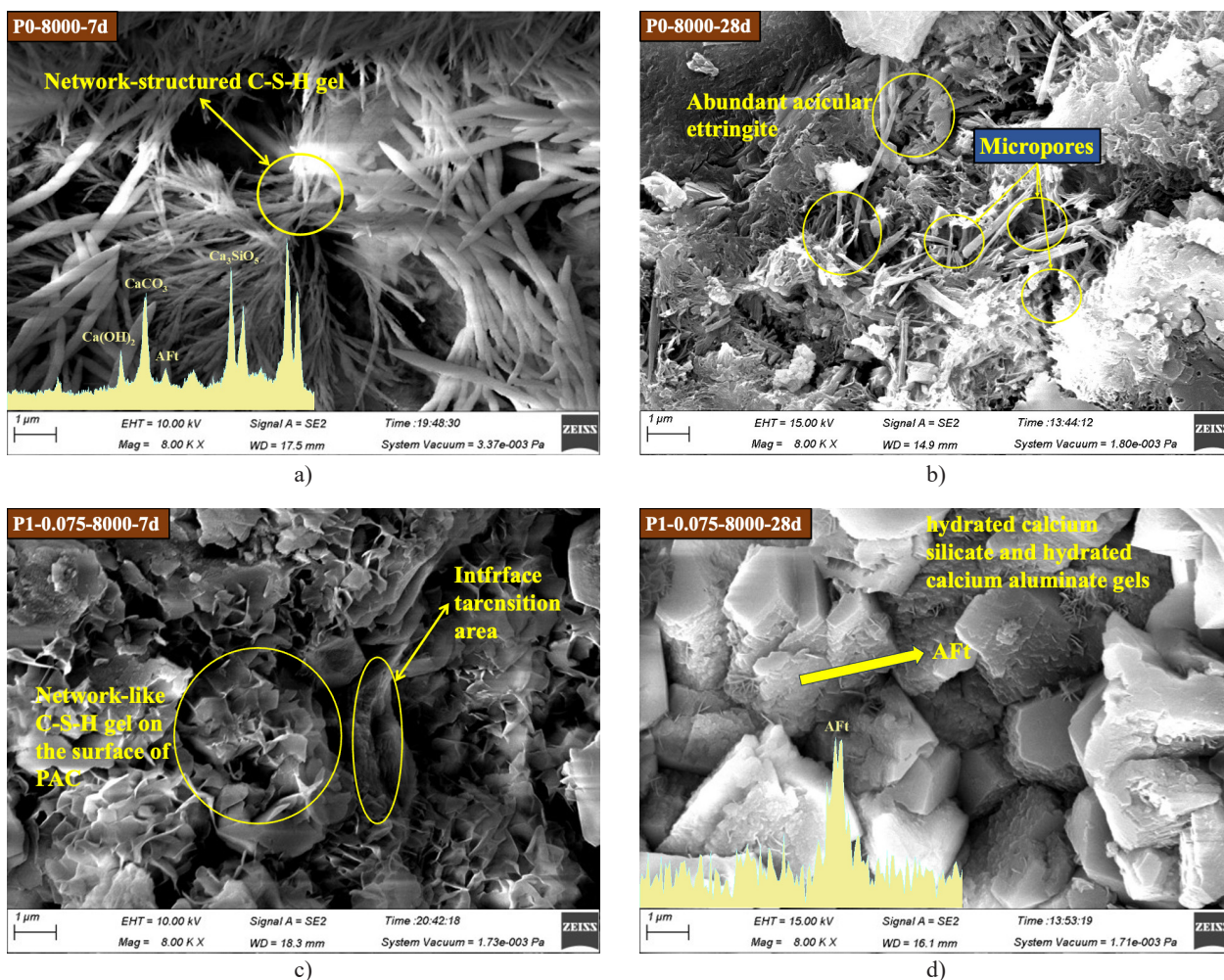


Figure 10. Microstructural evolution during hydration.

teristic of the cementitious matrices. Notably, no additional diffraction peaks were detected in the PAC-modified pastes, suggesting that the active components within the PAC residue primarily exist in an XRD-amorphous state and do not form new detectable crystalline phases. Consequently, the phase composition of the hydration products remains fundamentally consistent with cement replacement levels of up to 20 %.

Moreover, a closer examination of the relative intensities of the portlandite and C_3S characteristic peaks shows a negligible change among A0, A10, and A20 at 7 days, reflecting the limited early-age reactivity of the PAC residue. By 28 days, however, a discernible attenuation of the portlandite and alite peaks is observed in the PAC-modified pastes, attributable to the reduced cement dosage inherent to the replacement, which marginally lowers the absolute quantity of these phases, and the gradual onset of pozzolanic (volcanic ash) reactions consuming $\text{Ca}(\text{OH})_2$.

To further elucidate the microstructural and morphological differences engendered by the PAC residue addition, a subsequent scanning electron microscopy investigation was performed on the three paste groups.

Influence of the PAC residue content on the cement hydration process

To visualise the effect of the different PAC residue dosages on the cement hydration, the SEM images of the reference paste P0 (pure cement), P1 (10 % cement replaced by PAC residue), and P2 (20 % replacement) were analysed (Figure 10). In Figure 10a, the P0 micrograph shows abundant needle-like ettringite crystals along with minor microporosity. In Figure 10b, corresponding to the P1 mix, the amount of ettringite is reduced, and the small pores seem to be filled. This behaviour is due to both the lower Ca^{2+} concentration caused by the partial cement replacement and the gradual dissolution of Al_2O_3 in the PAC residue, which produces AlO_2^- ions; the increased AlO_2^- concentration in the solution prevents the formation of additional ettringite.

Table 3. Mix proportions of the paste samples.

Mix ID	Material quantity per unit volume (kg·m ⁻³)					
	Cement	Water	Coarse aggregate	Fine aggregate	PAC residue	Residue particle size
P0	360				0	-
P1	324	144	523.8	1222.2	36	0.075mm
P2	288				72	0.075mm

At a 20 % replacement level (P2), as illustrated in Figure 10c, the depletion of ettringite (AFt) becomes more pronounced. This phenomenon is attributed to the inherent thermodynamic instability of AFt in environments with elevated aluminium concentrations; the dissolution of Al₂O₃ from the PAC residue increases the Al/S ratio in the pore solution, thereby promoting the transformation of AFt into monosulfate (AFm). Although the substitution of cement with PAC residue reduces the overall volume of the primary hydration products, the PAC particles effectively function as micro-aggregates. These particles facilitate matrix densification through a physical filling effect, which partially mitigates the reduction in chemical binding products and helps maintain the microstructural integrity of the paste.

CONCLUSIONS

When the replacement level reaches 20 % (P2), as shown in Figure 10c, the depletion of ettringite becomes even more evident. Due to the relative instability of the ettringite phase, it tends to convert into monosulfate, a process that is further promoted by higher AlO₂⁻ concentrations. Although adding low to moderate amounts of PAC residue reduces the total amount of hydration products, the PAC particles serve as micro-aggregates that help maintain the matrix density at the microscale.

(1) With an increasing replacement ratio of cement by PAC residue, the compressive strength and freeze-thaw resistance of the static-pressed bricks progressively decrease. When the PAC residue replacement ratio reaches 10 – 20 %, both the compressive strength and freeze-thaw performance exhibit a pronounced decline.

(2) The incorporation of a moderate amount of PAC residue refines the microstructure of the matrix, enhancing its compactness. The low-level addition of PAC residue contributes to the densification of the cementitious matrix and effectively refines the pore structure. This synergistic effect of micro-filling and latent pozzolanic activity partially compensates for the mechanical performance loss in static-pressed concrete bricks resulting from the reduced cement clinker content.

(3) Considering the balance among the brick strength, freeze-thaw durability and resource utilisation of the residue, it is recommended that the replacement ratio of cement by PAC residue be limited to ≤ 15 %.

Acknowledgments

The authors received no specific funding for this research. We appreciate the constructive comments from the editorial team and anonymous reviewers.

REFERENCES

- Matsui Y., Shirasaki N., Yamaguchi T., Kondo K., Machida K., Fukuura T., Matsushita T. (2017): Characteristics and components of poly-aluminum chloride coagulants that enhance arsenate removal by coagulation: Detailed analysis of aluminum species. *Water Research*, 118, 177-186. doi: 10.1016/j.watres.2017.04.037
- Zhang X.W., Tong K., Lu L., Feng C.Y., Huang Z.S. (2024): Progress in Modification and Production Process Optimization of a Typical Water Treatment Flocculant (Polyaluminium Chloride). *Technology of Water Treatment*, 50(9), 20-25. doi: 10.16796/j.cnki.1000-3770.2024.09.004
- Hatamifar A., Gholikandi G.B. (2024): Synergistic effect of innovative bentonite and poly aluminum chloride (PAC) combination for excess and digested sludge thickening and dewatering. *Desalination and Water Treatment*, 317, 100131. doi: 10.1016/j.dwt.2024.100131
- Xia R., Liu W., Cao D., Wang N., Luo W., Nghiem L.D., Lin X. (2023): Comparison of different coagulants to improve membrane distillation performance for landfill leachate concentrate treatment. *Environmental Science: Water Research & Technology*, 9(5), 1934-1945. doi: 10.1039/D3EW00532A
- Zhang N., Yang Y., Fan L., Zheng X., Wang J., Jiang C., Xu S., Xu H., Wang D. (2023): Coagulation effect of polyaluminum-titanium chloride coagulant and the effect of floc aging in fluoride removal: A mechanism analysis. *Separation and Purification Technology*, 325, 124674. doi: 10.1016/j.seppur.2023.124674
- Wu Z., Zhang X., Pang J., Li J., Zhang P. (2020): High-poly-aluminum chloride sulfate coagulants and their coagulation performances for removal of humic acid. *RSC Advances*, 10, 7155-7162. doi: 10.1039/C9RA10189F
- Azhar A.A., Haron N.F., Ismail H.B. (2022): The Efficiency Assessment of Poly-Aluminium Chloride (PAC) in Water Treatment Plant Process: A Case Study at Sultan Iskandar Water Treatment Plant, Johor. *Journal of Sustainable Civil Engineering and Technology*, 1(2), 8-16. doi: 10.24191/

- jsctet.v1v2.8-16
8. Liu S., Zhuang X., Wang C. (2021): Application of Polyaluminium Chloride Coagulant in Urban River Water Treatment Influenced the Microbial Community in River Sediment. *Water*, 13(13), 1791. doi: 10.3390/w13131791
 9. Santos A.A.M., Cordeiro G.C. (2021): Investigation of particle characteristics and enhancing the pozzolanic activity of diatomite by grinding. *Materials Chemistry and Physics*, 270, 124799. doi: 10.1016/j.matchemphys.2021.124799
 10. Li Z., Gao Y., Zhang J., Zhang C., Chen J., Liu C. (2021): Effect of particle size and thermal activation on the coal gangue based geopolymer. *Materials Chemistry and Physics*, 267, 124657. doi: 10.1016/j.matchemphys.2021.124657
 11. Panwar N., Chauhan A. (2018): Optimizing the effect of reinforcement, particle size and aging on impact strength for Al 6061-red mud composite using Taguchi technique. *Sādhanā*, 43, Article 101. doi: 10.1007/s12046-018-0870-6
 12. Zeng Y., Wang Z., Pan Z., Shen L., Teng J., Lin H., Zhang J. (2023): Novel thermodynamic mechanisms of co-conditioning with polymeric aluminum chloride and polyacrylamide for improved sludge dewatering: A paradigm shift in the field. *Environmental Research*, 234, 116420. doi: 10.1016/j.envres.2023.116420
 13. Kim G., Ryu J., Ryu T., Kim H., Shin J., Cho D. (2024): Effects of calcination temperature on the adsorption ability of polyaluminum chloride (PAC) sludge-derived granules for As(V). *Journal of Water Process Engineering*, 57, 104688. doi: 10.1016/j.jwpe.2023.104688
 14. Li Q., Zhang J., Gao J., Huang Z., Zhou H., Duan H., Zhang Z. (2022): Preparation of a novel non-burning polyaluminum chloride residue (PACR) compound filler and its phosphate removal mechanisms. *Environmental Science and Pollution Research*, 29, 1532-1545. doi: 10.1007/s11356-021-15724-2
 15. Xu P., Yang H., Dong H., Ding Y., Yuhao C. (2022): The effects of polyaluminium chloride (PAC) slag on the properties of recycled concrete. *Ceramics - Silikáty*, 66(4), 419-427. doi: 10.13168/cs.2022.0037
 16. Hou D., Wu D., Wang X., Gao S., Yu R., Li M., Wang P., Wang Y. (2021): Sustainable use of red mud in ultra-high performance concrete (UHPC): Design and performance evaluation. *Cement and Concrete Composites*, 115, 103862. doi: 10.1016/j.cemconcomp.2020.103862
 17. Wang H., Liu X., Zhang Z. (2023): Pozzolanic activity evaluation methods of solid waste: A review. *Journal of Cleaner Production*, 402, 136783. doi: 10.1016/j.jclepro.2023.136783
 18. Yang W., Hou Z., He H., Xu P., Sun W., Wang Y., Gong J. (2022): Effect of particle size and dosing of polymeric aluminum chloride waste residue on cement mortar. *Geofluids*, 2022, Article ID 9675715. doi: 10.1155/2022/9675715
 19. Xu P., Zhang Z., Hou Z., Zheng M., Tong J. (2024): Influence of Polyaluminum Chloride Residue on the Strength and Microstructure of Cement-Based Materials. *Fluid Dynamics & Materials Processing*, 20(6), 1299-1312. doi: 10.32604/fdmp.2023.046183
 20. Zhang J., Li S., Li Z., Liu C., Gao Y. (2020): Feasibility study of red mud for geopolymer preparation: effect of particle size fraction. *Journal of Material Cycles and Waste Management*, 22, 1328-1338. doi: 10.1007/s10163-020-01023-4
 21. Shamaki M., Adu-Amankwah S., Black L. (2021): Reuse of UK alum water treatment sludge in cement-based materials. *Construction and Building Materials*, 275, 122047. doi: 10.1016/j.conbuildmat.2020.122047
 22. Pitarch A.M., Reig L., Tomás A.E., Forcada G., Soriano L., Borrachero M.V., Payá J., Monzó J.M. (2021): Pozzolanic activity of tiles, bricks and ceramic sanitary-ware in eco-friendly Portland blended cements. *Journal of Cleaner Production*, 279, 123713. doi: 10.1016/j.jclepro.2020.123713
 23. Shen W., Cao L., Li Q., Zhang W., Wang G., Li C. (2015): Quantifying CO₂ emissions from China's cement industry. *Renewable and Sustainable Energy Reviews*, 50, 1004-1012. doi: 10.1016/j.rser.2015.05.031
 24. He Z., Wang B., Shi J., Rong H., Tao H., Jamal A.S., Han X. (2024): Recycling drinking water treatment sludge in construction and building materials: A review. *Science of The Total Environment*, 926, 171513. doi: 10.1016/j.scitotenv.2024.171513
 25. Ahmadi M., Hakimi B., Mazaheri A., Kioumarsi M. (2023): Potential use of water treatment sludge as partial replacement for clay in eco-friendly fired clay bricks. *Sustainability*, 15(12), 9389. doi: 10.3390/su15129389
 26. Nie Y., Shi J., He Z., Zhang B., Peng Y., Lu J. (2022): Evaluation of high-volume fly ash (HVFA) concrete modified by metakaolin: Technical, economic and environmental analysis. *Powder Technology*, 397, 117121. doi: 10.1016/j.powtec.2022.117121
 27. Zhang S., Chen B., Tian B., Lu X., Xiong B. (2022): Effect of Fly Ash Content on the Microstructure and Strength of Concrete under Freeze-Thaw Condition. *Buildings*, 12(12), 2113. doi: 10.3390/buildings12122113
 28. Aygörmez Y. (2021): Performance of ambient and freezing-thawing cured metazeolite and slag based geopolymer composites against elevated temperatures. *Revista de la Construcción*, 20(1), 145-162. doi: 10.7764/rdlc.20.1.145
 29. Shpak A., Gong F., Jacobsen S. (2023): Frost durability of high-volume fly ash concrete: Relation liquid transport-damage. *Cement and Concrete Research*, 163, 107017. doi: 10.1016/j.cemconres.2022.107017
 30. Zhang Y., He Y., Cui X., Liu L. (2023): Enhancing Freeze-Thaw Resistance of Alkali-Activated Slag by Metakaolin. *ACS Omega*, 8(23), 20869-20880. doi: 10.1021/acsomega.3c01600